J Low Temp Phys (2010) 160: 219–239
DOI 10.1007/s10909-010-0189-0

Notes on Measurement Methods of Mechanical Resonators Used in Low Temperature Physics

P. Skyba

Received: 31 December 2009 / Accepted: 26 May 2010 / Published online: 22 June 2010

Abstract Mechanical resonators like vibrating wires, grids, spheres, torsional oscillators and recently introduced tuning forks are very useful experimental tools used for the study of various physical characteristics of cryogenic liquids and gases. As the information about the physical interactions of the resonator with surrounding fluid is carried by the voltage or current, the physical quantities being measured by some technique, it is obvious that the measurement electronics and electrical connections themselves affect the precision of the measurements. The aim of this contribution is to show: (i) how the electronic circuitry used for measurements of these resonators influences the precision of measurements, (ii) how this circuitry contributes to the background of the measurements, which may lead to incorrect physical interpretation, (iii) to highlight crucial aspects of the measuring techniques applied and (iv) perhaps to offer a general recipe on how to deal with the measurement techniques for these resonators.

Keywords Mechanical resonators · Vibrating wires · Tuning forks · Oscillating grids · Quantum turbulence

1 Introduction

Mechanical resonators like vibrating wires [1–4], torsional oscillators [5], vibrating spheres [6] and recently introduced tuning forks [7–11] are traditional experimental

P. Skyba (✉)
Centre of Low Temperature Physics, Institute of Experimental Physics, SAS and P.J. Šafárik University Košice, Watsonova 47, 04001 Košice, Slovakia
e-mail: skyba@saske.sk

P. Skyba
Department of Physics, University Lancaster, Lancaster, LA1 4YB, UK

tools used for cryogenic fluid investigations. Immersed in a fluid and brought into the forced oscillatory motion they interact with the fluid surrounding them. In a linear approximation, the motion of these mechanical resonators can be described by the very well know equation

$$\frac{d^2x}{dt^2} + \gamma \frac{dx}{dt} + \omega_0^2 x = F_0 \exp(i\omega t), \tag{1}$$

where the parameter F_0 describes the driving force amplitude normalized by the mass m. The second term in (1) characterizes the damping force (in units rad/sec) arising from the fluid that acts against the resonator motion and the intrinsic damping due to internal mechanical friction of the resonator. Here it is assumed that the damping force is linear with the resonator velocity v with damping constant γ ($\gamma = \gamma_2 + i\gamma_1$). γ_2 refers to the dissipative component of the damping force. γ_1 characterizes the reactive component associated with the fluid backflow around the resonator and effectively gives the resonator a greater mass. The last term in (1) characterizes the restoring force of the resonator, where ω_0 is the resonator's resonance frequency in vacuum.

In the solution to (1), the velocity v at which the resonator moves through the fluid depends on the frequency and amplitude of the driving force and on the properties of the fluid (expressed by the constant γ) as

$$v(\omega) = v_0 \frac{\gamma_2^2\omega^2 + i\gamma_2\omega(\omega_0^2 - \omega^2 - \gamma_1\omega)}{(\omega_0^2 - \omega^2 - \gamma_1\omega)^2 + \gamma_2^2\omega^2}, \tag{2}$$

where v_0 is the maximum velocity amplitude at the resonance frequency ω_{R0} and depends on the driving force amplitude F_0. The resonance frequency ω_{R0} can be calculated from the expression $\mathrm{Im}[v(\omega)] = 0$. The motion of resonators with velocity v is associated with the generation of an electric signal—a voltage or a current in relation with their principle of operation, and the magnitude of the voltage or current is proportional to the velocity of the resonator motion. The proportionality constant has to be determined from experiment.

Mechanical resonators used traditionally may be split into two groups according to the type of signal produced, that is either voltage or current. Vibrating wires are typical example belonging to the first group, while the torsional oscillators, electrostatically driven grids and tuning forks are examples of the second one. In the first part, an analysis of measurement techniques used for vibrating wire detection without and with low temperature signal transformer is presented. The current measurement techniques applied to tuning fork and torsional (grid) oscillators are discussed in the second part. We present theoretical models based on circuit analysis and these are compared with the experimental reality.

2 Vibrating Wires—Direct Measurements

A vibrating wire is usually made of either a superconducting single wire (Ta) or a single filament from a multi-filament wire (NbTi), bowed into a semicircle of radius

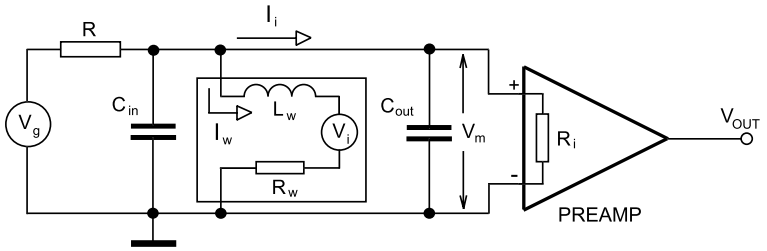

Fig. 1 Schematic electric connection of a typical circuit used for vibrating wires measurements. The vibrating wire is modelled using an inductance L_w and a resistor R_w. A voltage source V_i (see (3)) models the induced voltage generated by the wire oscillation in the magnetic field

R (or other shape e.g. rectangular) immersed in the fluid. With the aid of a steady magnetic field $\mathbf{B}_0$ oriented in the plane of the wire loop and an ac-current I_w flowing through the wire, the wire is driven into mechanical resonance as a consequence of the Lorentz force. The wire's harmonic motion cuts the magnetic flux resulting in an induced voltage generation with amplitude

$$V_i(\omega) = kB_0 l v(\omega). \tag{3}$$

Here $v(\omega)$ is given by expression (2), l denotes the spacing between the wire posts (usually $l = 2R$ for a semicircular wire loop) and k is a constant characterizing the shape of the wire (for semicircular wire loop $k = \pi/4$). The driving force F_D acting on the semicircular wire loop has the tendency to bend the wire, which is fixed in two points. These points determine the wire oscillation axis. The driving force amplitude can be obtained from the expression for a torque

$$|\mathbf{M}_D| = \int |\mathbf{d} \times (I_w d\mathbf{s} \times \mathbf{B_0})| = B_0 I_w R^2 \int_0^{\pi} \sin^2\phi d\phi = \frac{\pi}{4} B_0 I_w l R, \tag{4}$$

where $ds = Rd\phi$, $\mathbf{d}$ is the vector which denotes the distance between the wire oscillation axis and the element $d\mathbf{s}$ on the wire and its absolute value can be expressed as $d = R\sin\phi$. Equation (4) determines the driving force amplitude as $F_D = kB_0 I_w l$, where k is above mentioned constant assuming that the distance between the wire oscillation axis and the driving force F_D is R.

A typical experimental setup used for the measurement of the induced voltage V_i generated by the vibrating wire motion is presented in Fig. 1. It consists of a generator providing a harmonic excitation voltage V_g being converted to a current I using a resistor R ($R \sim 1$ kΩ–1 MΩ). The current I_w flowing through the vibrating wire generates a harmonic magnetic field. Thus, the vibrating wire can be modelled as a self inductance L_w ($\Phi_w \sim L_w I_w$). The induced voltage V_i (see expression (3)) can be modelled as a harmonic voltage source. The voltage V_i is measured by a differential preamplifier (usually a part of the lock-in amplifier) having an input resistance R_i ($R_i \sim 10$ MΩ). To measure V_i a four wire configuration is used. The two ends of the vibrating wire are spot welded to superconducting pads or simply soldered to the measuring leads (cables). We may introduce a normal resistance of the wire which can be modelled by a resistor R_w. As the vibrating wires often are made of type

II superconductors, application of a high magnetic field may also cause a nonzero resistance R_w of the vibrating wire. Finally, capacitors C_{in} and C_{out} represent the capacitance of the input and output leads (or cables), respectively, which are used for the vibrating wire connection. As they are connected in parallel, then $C = C_{in} + C_{out}$. We assume that the cable resistances can be neglected, being small in comparison to R and R_i. As Fig. 1 shows, there are two voltage sources acting in this circuitry (V_g and V_i). Using the superposition theorem, the circuit can be analyzed in terms of two impedances $Z_1(\omega)$ and $Z_2(\omega)$, each the combination of individual circuit elements (R_w, L_w, C, R, R_i (see below)). Clearly, the voltage V_m measured by a differential preamplifier can then be expressed as

$$V_m(\omega) = \frac{Z_1(\omega)V_g(\omega)}{R + Z_1(\omega)} + \frac{Z_2(\omega)V_i(\omega)}{R_w + i\omega L_w + Z_2(\omega)} = V_{bgrd}(\omega) + V_{im}(\omega). \quad (5)$$

The measured voltage $V_m(\omega)$ consists of two terms: the first one, V_{bgrd} is the background voltage generated by the current flow through the wire, and the second one, V_{im} is the induced voltage generated due to the wire motion in the magnetic field. The contribution of the background voltage to V_m is calculated assuming that $V_i = 0$ volts. Then, the admittance $Y_1 = 1/Z_1$ can be expressed as

$$Y_1 = \frac{R_w - i\omega(CR_w^2 - L_w)}{R_w^2 + \omega^2 L_w^2}. \quad (6)$$

In the derivation a term $\omega^2 L_w C$ determining the electrical resonance frequency of L_w-C circuit was neglected because this term is very small in the frequency range of interest i.e. the mechanical resonance frequency of the wire. Ratios R_w/R_i and $\omega L_w/R$ were also omitted being negligibly small. Substituting expression (6) into the first term of (5) and after a short manipulation one gets the expression for background voltage

$$V_{bgrd}(\omega) = \frac{V_g(\omega)}{R}\left(R_w + i\omega(CR_w^2 - L_w)\right). \quad (7)$$

The vibrating wire resistance R_w is responsible for a non-zero value of the in-phase component, while the capacitance C of the cable and the vibrating wire inductance L_w generate the quadrature component of the background voltage V_{bgrd}. The second term, the induced voltage V_{im}, as a result of the harmonic motion of the wire in the magnetic field, can be written in the form

$$V_{im}(\omega) = \left[1 - i\omega(R_w C + L_w/R')\right] V_i(\omega), \quad (8)$$

where $R' = R\,R_i/(R + R_i)$ and if $R \ll R_i$, then $R' \approx R$. For typical experimental setup $\omega L_w/R' \gg \omega R_w C$ is valid assuming that $R_w \to 0\ \Omega$, substituting expressions (7) and (8) into (5), the voltage V_m measured by the lock-in amplifier can be expressed as

$$V_m(\omega) = \frac{V_g(\omega)}{R}(R_w - i\omega L_w) + V_i(\omega)\left(1 - \frac{i\omega L_w}{R'}\right), \quad (9)$$

where $V_i(\omega) \sim B_0 l v(\omega)$ and $v(\omega)$ is given by (2). As it follows from (9), the contribution of the excitation voltage V_g to the measured signal V_m is obvious. The non-zero

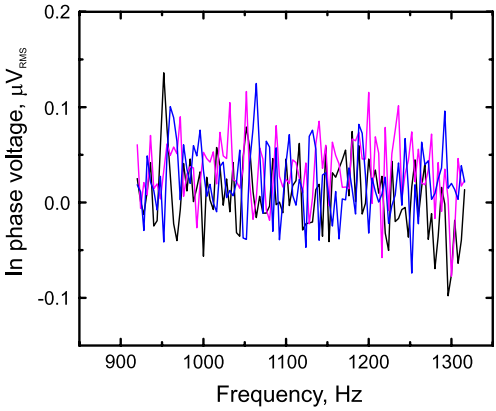

Fig. 2 (Color online) The frequency dependence of the in phase component of the voltage V_m measured for various excitation voltages V_g (for 5, 15 and 25 mV_{RMS}) in zero magnetic field

resistance of the vibrating wire R_w contributes to the in-phase component, while the self inductance of the wire L_w contributes to the quadrature component of the measured signal V_m. The induced voltage V_i is usually the dominant part of the measured signal V_m. However, there is also an additional, mixed contribution to V_m due to the wire self inductance L_w, when the in-phase (real) part of V_i contributes to the quadrature (imaginary) part of V_m and, vice versa, the imaginary part of V_i adds to the real part of V_m. These mixed contributions are of the order of $\omega L_w/R'$, which are usually very small due to high value of R' and normally they may be neglected.

3 Direct Wire Measurements—Experimental

Comparison of the theoretical model with experimental data was performed using a standard NbTi superconducting wire of diameter of 13 μm and loop radius 2 mm. Each end of the vibrating wire was spot welded to a niobium foil together with another two single filament NbTi wires, thus providing superconducting joints and allowing the four wire measurement. The vibrating wire was placed in an experimental cell made of Stycast. The induced voltage generated by the vibrating wire was measured using the technique described above. The wire vacuum resonance frequency was 1270 Hz and the frequency width of the resonance in vacuum i.e. the intrinsic width was 0.5 Hz.

The frequency dependence of the absorption (in-phase) component of the V_{bgrd} measured at temperature of 0.9 K and zero magnetic field for various excitations is presented in Fig. 2. As can be seen, the wire resistance $R_w \rightarrow 0\ \Omega$ since there is no dependence on the excitation voltage V_g detected, we can conclude that the measured voltage corresponds to the noise level. When $R_w \neq 0\ \Omega$, a linear dependence of the in phase voltage component on the excitation V_g will be detected, from which the value of the wire resistance R_w can be determined.

The frequency dependence of the quadrature component of the background voltage measured at various excitations and zero external magnetic field is presented in Fig. 3. Having the vibrating wire in the superconducting state i.e. $R_w \rightarrow 0\ \Omega$ and

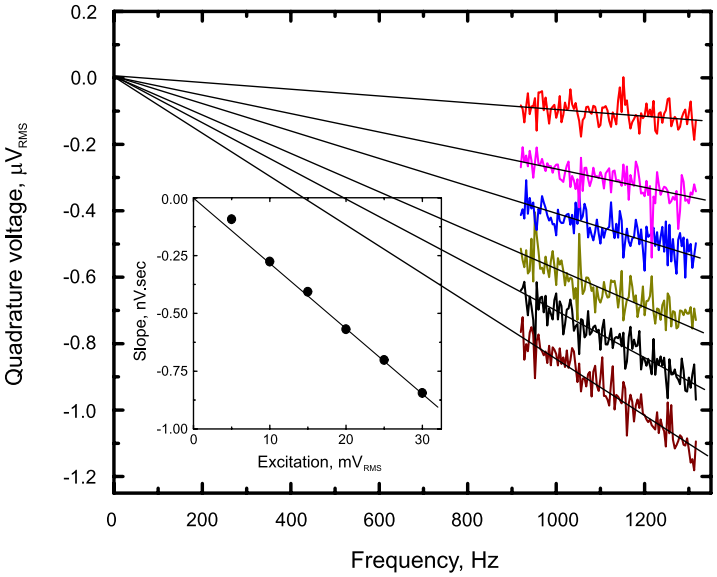

Fig. 3 (Color online) Frequency dependence of the quadrature component of the voltage V_m measured at various excitation voltages V_g (from top to bottom for 5, 10, 15, 20, 25 and 30 mV_{RMS}) in zero magnetic field. The *lines* represent the fit to the experimental data of (10). The *inset* shows the dependence of the slope as a function of the excitation voltage V_g. For details see text

$B = 0$ T, then from (9) for the measured voltage V_m we get

$$V_m(\omega) = -i\omega \left(\frac{L_w}{R}\right) V_g(\omega). \tag{10}$$

Thus, while the in-phase component of V_m should stay constant and equal to the noise voltage, the imaginary (quadrature) component, according to the model, should vary linearly with the frequency and for various excitations V_g, the slope of the dependence $(L_w/R)V_g$ has to be different. In Fig. 3, the lines represent the fits to the experimental data using (10). It is obvious from (10) that for $\omega \to 0$ rad/sec, the measured voltage $V_m \to 0$ volts as well. The inset to Fig. 3 shows the dependence of the slopes $(L_w/R)V_g$ for the different excitations. This dependence allows the wire self inductance L_w to be determined knowing the value of the resistor R ($R = 1$ kΩ in our measurements). For the particular wire shown, the wire self-inductance L_w was found to be 44 nH. This value is order of magnitude larger than expected just from the semicircular loop of the wire itself. One should point out that it is not only the semicircular part of the wire which contributes to the wire self inductance, but also the adjacent leads of the vibrating wire forming the loop. To reduce the value of the vibrating wire self inductance, the leads to the vibrating wire should be tightly twisted together as close as possible to its active length. Based on the values of L_w and R we can estimate a correction for V_i to the measured signal V_m (the second term in (9)) due to the term $\omega L_w/R$ as $R \ll R_i$. This correction is of the order of 4.10^{-7} and is very small compared to 1 and can be neglected.

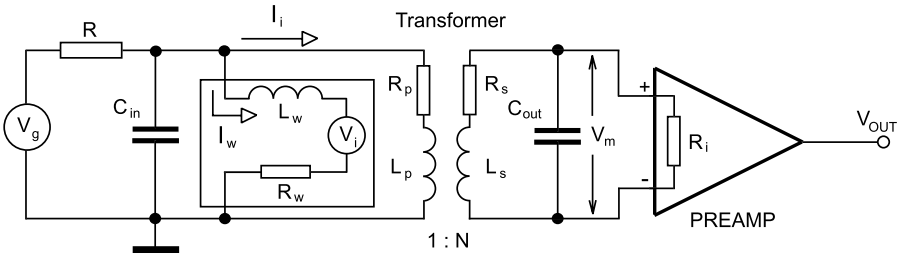

Fig. 4 Schematic electric connection of a typical circuit used for vibrating wires measurements including a signal transformer used for amplifying the induced voltage V_i (see text for details)

4 Vibrating Wires and Transformers

In superfluid ^{3}He-B at very low temperatures the dominant scattering process of the quasiparticles from the vibrating object is Andreev reflection [1]. To reduce the impact of this on the damping of the vibrating wire motion in superfluid ^{3}He-B and thus to keep the response in a linear regime, the wires are driven at very low velocities. Therefore, the corresponding induced voltage V_i is very small. For a preamplifier amplifying this signal at room temperature, its own noise voltage is of the same order as that being detected from the wire motion. To improve the signal to noise ratio, a low temperature transformer may be connected between the wire and preamplifier. Another possible way is to use a SQUID and a preamplifier to measure the vibrating wire response [12, 13]. The transformer amplifies the measured signal on the one side, however, on the second one has also some negative effects on the electronic characteristics of the detecting circuitry. A typical scheme of such a detection circuitry with transformer is shown in Fig. 4.

In Fig. 4, $1 : N$ is the gain of an ideal transformer, R_p and L_p denotes the resistance and inductance of the primary winding, respectively, while R_s and L_s denote these for the secondary winding. The mutual inductance of the transformer $M \sim \sqrt{L_p L_s}$ is assumed to be frequency independent in the range of frequencies of a few kHz, the frequency range of oscillations of the standard vibrating wires. Capacitors C_{in} and C_{out} model the capacitances of the input and output coaxial cables, respectively. The transformer is modelled using a standard "T" model. The vibrating wire is simulated in the same way, that is, as an inductance L_w and a resistance R_w, together with a voltage source V_i.

The voltage V_m being measured by the lock-in amplifier is again the superposition of two voltages

$$V_m(\omega) = V_{bgrd}(\omega) + V_{im}(\omega). \tag{11}$$

Looking at Fig. 4, one can expect the existence of a resonance of the secondary winding of the transformer at frequency $\omega_s = 1/\sqrt{L_s C_{out}}$. However, the inductance of the secondary winding of commercially available low temperature signal transformers [14] is enormous, it is of the order of hundreds of henry due to the transformer core. Therefore, the resonance frequency of the secondary winding, for typical values of capacitance C_{out} is of the order of tens of hertz, well below the wire resonance frequency. Analysis shows that the mutual inductance M and capacitance C_{in} determine

the resonance frequency of the 'primary side' of the transformer $\omega_p = 1/\sqrt{MC_{in}}$. Therefore, we may assume that the vibrating wire resonance frequency $\omega_0 \ll \omega_p$ and that $R_i \gg R_s$ and also that $R_i/N^2 \gg \omega M$ in absolute values are satisfied. As a result of these assumptions, we need to take into account only the impedance of the 'primary' side of the transformer including the mutual inductance M. Then by applying the superposition theorem, as above, one can obtain an expression for the background voltage in the form

$$V_{bgrd}(\omega) = N\frac{V_g(\omega)}{RR_p}\left[R_w R_p + \omega^2 L_w(L_p + M) - i\omega L_w R_p\right]. \tag{12}$$

As can be seen from (12), in contrast to the direct measurement of the wire, where the in-phase component does not show a frequency dependence (in the framework of the model presented) the presence of the transformer introduces a ω^2 term. The frequency dependence of the quadrature component stays the same as for the direct wire measurement. If there is no transformer present, that is, if $N = 1$, $R_p = 0$, $L_p = M = 0$, then expression (12) reduces to

$$V_{bgrd}(\omega) = \frac{V_g(\omega)}{R}\left(R_w - i\omega L_w\right), \tag{13}$$

which is the same as the background voltage contribution in expression (9).

The second term in (11) can be derived in the form

$$V_{im}(\omega) = N\left[1 - \frac{i\omega^3 R(L_p + M)^2 L_w}{(RR_p)^2 + \omega^2 R^2(L_p + M)^2}\right]V_i(\omega). \tag{14}$$

In the derivation of (14) the terms $R_w(R + R_p)$ and $i\omega M R_w$ were neglected being small in comparison with other terms assuming that $R_w \to 0\ \Omega$. Expression (14) again shows that the voltage amplitude V_{im} being measured by preamplifier is less than the induced voltage V_i due to the wire self-inductance L_w. One can consider a limiting case when $R_p \ll \omega(L_p + M)$. This case results in

$$V_{im}(\omega) = NV_i(\omega)\left(1 - \frac{i\omega L_w}{R}\right), \tag{15}$$

which together with (13), if $N = 1$, gives the same result as (9). In the second limiting case with transformer, if $R_p \gg \omega(L_p + M)$, one can get

$$V_{im}(\omega) = NV_i(\omega)\left(1 - \frac{i\omega^3(L_p + M)^2 L_w}{RR_p^2}\right), \tag{16}$$

here in both cases the $V_i(\omega)$ is given by expression (3).

If the wire resonance frequency ω_0 does not satisfy the condition $\omega_0 \ll \omega_p$, then one can expect a nontrivial frequency dependence of the background voltage because the wire resonance response will be overlapped by the resonance response of the transformer. This may easily happen especially when a higher transformer gain is used. In general, the higher the transformer gain, the lower the transformer resonance

frequency. One should also keep in mind that the application of the higher transformer gain is paid by the lowering of the input impedance R_i of the preamplifier by factor of $1/N^2$, which may also lead to the condition $\omega M \ll R_i/N^2$ not being satisfied. Then, the results presented above will not be valid and a frequency dependence of the secondary part of the transformer will affect the frequency dependence of the background voltage. Selection of the transformer gain is a compromise between the value of the signal to noise ratio and complications with the frequency response of the background contribution to the measured voltage from the circuitry.

5 Vibrating Wires and Transformers—Experimental

Below we compare the theoretical model described above with experiments performed using a standard NbTi superconducting wire of diameter 4 μm and loop radius of 2 mm. The wire resonance frequency in vacuum was 1100 Hz and intrinsic width of the resonance curve was 0.2 Hz. The wire was connected to the lock-in preamplifier via a low temperature transformer immersed in liquid ^{4}He and with a gain $N \sim 30$. The background signal was measured at zero magnetic field and at $T = 4$ K. In Fig. 5 the frequency dependencies of the in-phase component of the background voltages measured for various excitations are presented. The frequency dependencies confirm the quadratic frequency dependence of the in-phase component predicted by the model (see expression (12)). These measured dependencies allow the parameters R_w/R and $L_w(L_p + M)/(RR_p)$ to be determined. Inset to Fig. 5 shows the expected linear dependence of the slopes $NV_gL_w(L_p + M)/(RR_p)$ as a function of the excitation voltage V_g.

The frequency dependence for the quadrature component of the background voltage measured at the same excitations as that for the in phase component are presented in Fig. 6. The measured linear frequency dependencies of the quadrature component support the model presented above. Inset to Fig. 6 shows the dependence of the slopes (NV_gL_w/R) on excitations V_g. This dependence allows the wire self inductance L_w from the value of the slope (NL_w/R) to be determined, knowing the value of the resistor R and the gain of the transformer N.

The ratio of the coefficients $NL_w(L_P + M)/(RR_p)$ and (NL_w/R) (see expression (12)) and insets to Fig. 5 and Fig. 6 determine the value of $(L_p + M)/R_p$ straightforwardly. For this particular measurement presented it is 2×10^{-4} sec. Using this value together with the value of L_w/R one can calculate the influence of the wire self-inductance on the measured voltage V_{im}. The expression (14) can be rewritten in the form

$$V_{im}(\omega) = N\left[1 - i\frac{\omega L_w}{R}\frac{\omega^2A^2}{1+\omega^2A^2}\right]V_i(\omega), \tag{17}$$

where $A = (L_p + M)/R_p$. As $A = 2 \times 10^{-4}$ sec and the wire angular resonance frequency is $\omega \sim 10^4$ rad/sec, the second term in the imaginary fraction is of the order of unity and the influence is determined by $\omega L_w/R$. In this case, the value of L_w/R determined form the background measurement is $L_w/R \sim 4 \times 10^{-10}$ sec and hence, the measurement error due to the wire self-inductance is of the order of

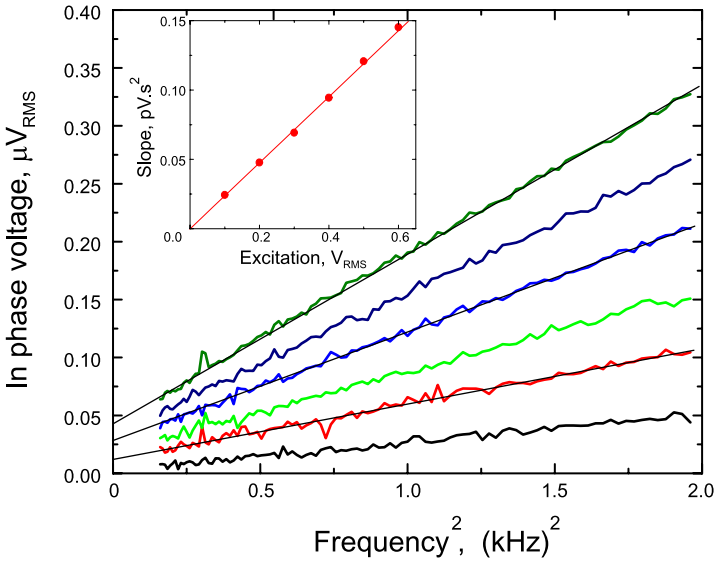

Fig. 5 (Color online) Frequency dependence of the in phase component of the voltage V_m measured at various excitation voltages V_g (from 100 to 600 mV_{RMS} in 100 mV_{RMS} steps in zero magnetic field. The *lines* represent the fit to the experimental data of (12). The *inset* shows dependence of the slopes as a function of excitation voltage V_g from which the value of $(L_p + M)/R_p$ can be determined (for details see text)

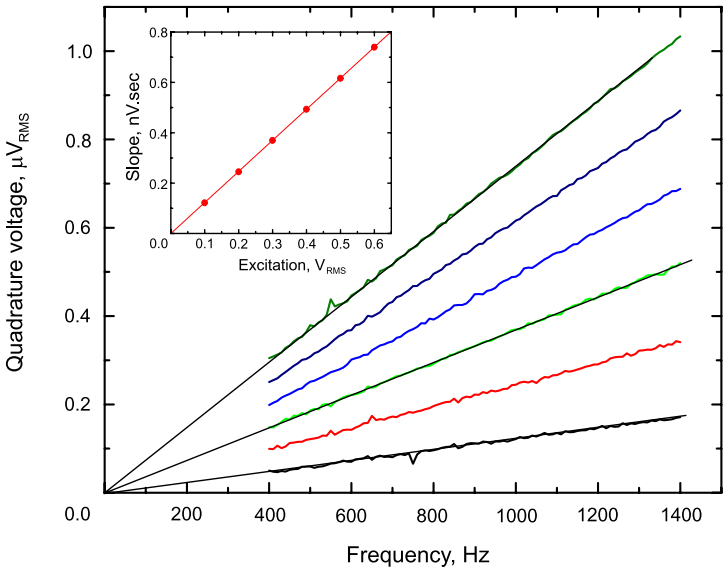

Fig. 6 (Color online) Frequency dependence of the quadrature component of the voltage V_m measured at various excitation voltages V_g (from 100 to 600 mV_{RMS} in 100 mV_{RMS} steps) in zero magnetic field. The *lines* represent the fit to the experimental data by (12). The *inset* shows dependence of the slopes as a function of excitation voltage V_g from which the value of L_w can be determined

4×10^{-6}. The error is very small and in majority of cases can be neglected, however, one should always estimate its magnitude.

On the other hand, the parameters N, R_w, L_w, R_p and $L_P + M$ affect the frequency dependence of the background voltage being especially important when broad frequency sweeps of the vibrating wire are measured. Once these parameters are determined from experiment, one obtains a complete knowledge about the background signal contribution to the measured signal. This background contribution can easily be subtracted from the measured signal in order to get the net signal from the vibrating wire.

6 Tuning Forks

In contrast to vibrating wires, where the induced voltage provides information about the interaction of the wire with the surrounding fluid modelled through γ coefficient, in the case of a tuning fork it is an electric current. The fork motion is described by the same as for the wire (1), however, the right side is equal to the electric part of the Lorentz force $F_0 = nqE/m$, instead of the magnetic part

$$\frac{d^2x}{dt^2} + \gamma \frac{dx}{dt} + \omega_0^2 x = F_0 \exp(i\omega t), \tag{18}$$

where E is the electric field intensity, n is the number of atoms with charge q and ω_0 is the fork resonance frequency in vacuum usually well defined by the forks producers. The electric field polarizes atoms and results in the crystal lattice deformation manifested in the form of the prong displacement. The magnitude of this displacement depends on the interaction of the fork with the surroundings (neglecting its intrinsic damping) and this sets the amplitude of the polarization p. Periodic changes of the electric field E produce a periodic time variation of the polarization p, that is a displacement current I_F flowing through the fork. This current amplitude is proportional to the electric field E amplitude and to the rate of displacements i.e. to the velocity of the prongs $v(\omega)$

$$I_F(\omega) = d_{11} E v(\omega) = \alpha v(\omega), \tag{19}$$

where d_{11} is the relevant component of the piezoelectric modulus tensor, α is the proportionality constant which needs to be determined experimentally [8] and $v(\omega)$ is given by expression (2). The magnitude of the driving force acting on the fork per prong is given by [8]

$$F_{TF} = \frac{\alpha V_{TF}}{2}, \tag{20}$$

where V_{TF} is the applied voltage across the tuning fork.

A typical measurement setup to measure the tuning fork is presented in Fig. 7. The output voltage V_o from the I/V converter (which may be built-in inside the lock-in amplifier) is then measured by a lock-in amplifier having the reference signal from the generator providing the excitation. The fork is excited by a harmonic voltage V_g

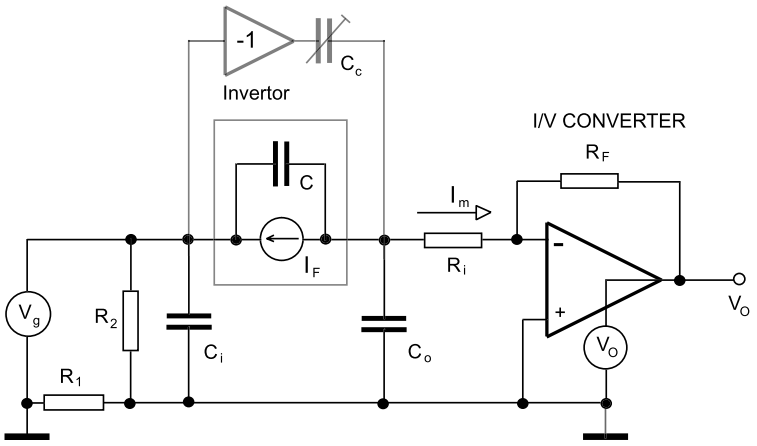

Fig. 7 Schematic electric connection of a typical circuit used for tuning forks measurements. The tuning fork is modelled as a frequency dependent current source I_F (see expression (19)). A compensation circuit drawn by the grey lines serves to suppress the quadrature component of the background voltage (for details see text)

supplied from a high resolution generator (including attenuation). The fork is modelled by a frequency dependent current source I_F (see (19)). The amplitude of I_F depends on the driving force amplitude and damping originating from the resistance of the fluid against the fork motion. The current source I_F is shunted by the capacitor C, which models a shunt capacitance created due to the presence of the metal electrodes on the fork surface. Capacitances of the input and output coaxial cables are labelled C_i and C_o. A divider formed by two resistors R_2 and R_1 models a possible problem with the ground potential of the generator which may be different than that of the I/V converter due to improper cables connections (it happens very often). This may lead to an additional offset appearing in the measurements (see below). Finally, R_F denotes the I/V converter feedback resistor providing the current amplification and R_i refers to the input resistance (impedance) of the I/V converter. We shall also assume that the current to voltage converter has a constant frequency-independent response in the frequency range of interest.

It is worth to mention at this point that the input resistance R_i of an ideal I/V converter is equal to zero, while in reality it is a few mΩ. However, the commercial I/V converters, like those built-in to the lock-in amplifiers may have an input resistance of the order of 1 kΩ. As we shall see below, the finite input resistance R_i of such I/V converters affects the precision of the current measurements.

As Fig. 7 shows, the output voltage amplitude V_o, similar to that for the wire, consists of two contributions

$$V_o(\omega) = V_{bgrd}(\omega) + Z(\omega)I_F(\omega) = V_{bgrd}(\omega) + V_{sig}(\omega). \tag{21}$$

The first term is the background voltage generated due to a 'leakage' of the current supplied from the generator to the input of the I/V converter. The second term is the signal voltage generated by the current I_F multiplied by an impedance $Z(\omega)$ characterizing the influence of the circuitry on the output voltage.

Using the superposition theorem one can derive the contribution of the background voltage V_{bgrd} in the form

$$V_{bgrd} = -\frac{Z_2}{R_1 + Z_2} \frac{1}{1 + \omega^2 C_o^2 R_i^2} \left(\omega^2 R_F R_i C C_o - \frac{R_1}{Z_2} + i\bar{k}\omega R_F C \right) V_g(\omega), \quad (22)$$

where $\bar{k} = 1 - R_1 C_o/(Z_2 C)$ and $Z_2 = R_2/(1 + i\omega R_2 C_i)$.

The second term in expression (21) i.e. the signal voltage V_{sig} generated due to the current I_F may be expressed in the form

$$V_{sig}(\omega) = -\frac{1 - i\omega C_o R_i}{1 + \omega^2 C_o^2 R_i^2} R_F I_F(\omega) = -R_F I_m(\omega), \quad (23)$$

assuming that $C \ll C_o$. From both expressions (22) and (23) it immediately follows what one should take care of in order to reduce the influence of the background voltage on V_o and to improve the precision of the measurements. First of all, one should use a proper I/V converter having input resistance $R_i \to 0\ \Omega$. Secondly, one should eliminate the potential difference between the generator and the I/V converter i.e. $R_1 \to 0\ \Omega$, so that $k \to 1$. Then, the I/V converter output voltage V_o measured by the lock-in amplifier can be expressed as

$$V_o(\omega) = -R_F I_F(\omega) - i\omega R_F C V_g(\omega). \quad (24)$$

Thus, if $R_i \to 0\ \Omega$, the potential of the fork output coax-cable is at virtual zero and therefore, there is zero voltage drop across the output capacitance and no current flows through it. However, if $R_i \neq 0\ \Omega$ the current flowing through the non-zero input resistance of the I/V converter generates a voltage drop also across the output capacitor C_o, which leads to a current leakage through C_o thus reducing the amplitude of the current being measured. Typically the capacitance of the output cable is of the order of 1 nF and (commercial) I/V converter input resistance is about $R_i \sim 1\ \text{k}\Omega$, so at a fork frequency $\omega/2\pi \sim 33000$ Hz the absolute amplitude of the current measured is reduced by 2.1 %.

A non-zero input resistance of the I/V converter will affect the determination of the α constant and the value of the driving force F_{TF} because both values depend on the voltage across the tuning fork V_{TF}, which in this case will not be the same as the excitation voltage V_g. The voltage across the tuning fork can be expressed as

$$V_{TF}(\omega) = \frac{Z_2}{R_1 + Z_2} V_g(\omega) - R_i I_m(\omega), \quad (25)$$

where I_m is the current being measured by the lock-in amplifier and this value also depends on C_0 (see expression (23)). At the fork resonance frequency ω_0, the error of the measurement can be estimated as $R_{TF}/(R_{TF} + R_i)$, where R_{TF} represents the fork damping in terms of an electric resistance. For a high Q-value resonance ($Q \sim 10^5$–10^6), when the fork is lightly damped, the value of R_{TF} is of the order of few kΩ and the error on the V_{TF} determination can easily be 10–30%. This may explain the differences in the values of α for forks of the same size measured in different laboratories. Another aspect of the I/V converter non-zero input resistance is

the nontrivial frequency dependence of the background voltage V_{bgrd} (see expression (22)).

Let us discuss the influence of the potential difference between the generator and the I/V converter. There are two possible limits: (i) $R_2 \ll 1/(\omega C_i)$ and opposite to the previous one (ii) $R_2 \gg 1/(\omega C_i)$.

In the first case $Z_2 \simeq R_2$ and two resistors R_1 and R_2 form a voltage divider. As a result, there will be a difference in voltage potentials between the generator and the I/V converter which causes a frequency independent positive shift of the I/V converter output voltage and also will reduce the magnitude of the fork excitation signal by a factor of the order of $R_2/(R_1 + R_2)$.

In the second case, a divider made of the impedance $1/(i\omega C_i)$ and the resistor R_1 is formed. As a result, one can expect to have a frequency dependence of both: (i) the potential difference between the generator and the I/V converter reference and (ii) also the frequency dependence of the magnitude reduction of the fork excitation signal. The order of the potential difference amplitude and the order of the excitation signal magnitude reduction can be expressed as $R_1/(1 + i\omega C_i R_1)$, and $1/(1 + i\omega C_i R_1)$, respectively. Correct grounding of the coax cables and measurement wires should set $R_1 \to 0\ \Omega$ and it should eliminate the problems discussed above.

Finally, let us turn our attention back to expression (24). According to this expression, there is only a background contribution to the quadrature component due to the presence of the parasitic (shunt) capacitance. This capacitance bypasses the current flowing from the generator and gives rise to the amplitude of the quadrature component especially, when the tuning fork is highly damped. However, in contrast to the vibrating wire case where it is practically impossible to eliminate the background voltage generated due to the wire self-inductance, it is not so for the tuning fork. In principle, one can compensate the quadrature background voltage using a transformer connected into a bridge [15]. Another, straightforward technique to compensate the quadrature component is based on an operational amplifier application working as an invertor (see Fig. 7). The invertor generates a compensation signal being derived directly from the fork excitation voltage signal by inverting it. Once a variable capacitance C_C connected to the invertor output is adjusted to the value of the order of the fork capacitance C, the invertor will supply the I/V convertor with a current of the same order of magnitude as that flowing through the fork capacitance C, but being opposite in phase they will compensate each other. This addition allows one to measure both signal components with good precision, even in the case of a strongly damped fork motion.

7 Tuning Forks—Experiment

In contrast to the vibrating wire, where one can easily determine the voltage backgrounds (in zero magnetic field), it is not the case for the tuning fork. The best way to determine the basic features of the fork measurement circuitry and background voltage contribution to the fork signal is to measure it in vacuum and at very low temperatures. The properly made and installed fork should have a high Q-value of the order of 10^5–10^6 (or even higher). The high Q-value allows the frequency dependence of the background voltage contribution to be determined experimentally

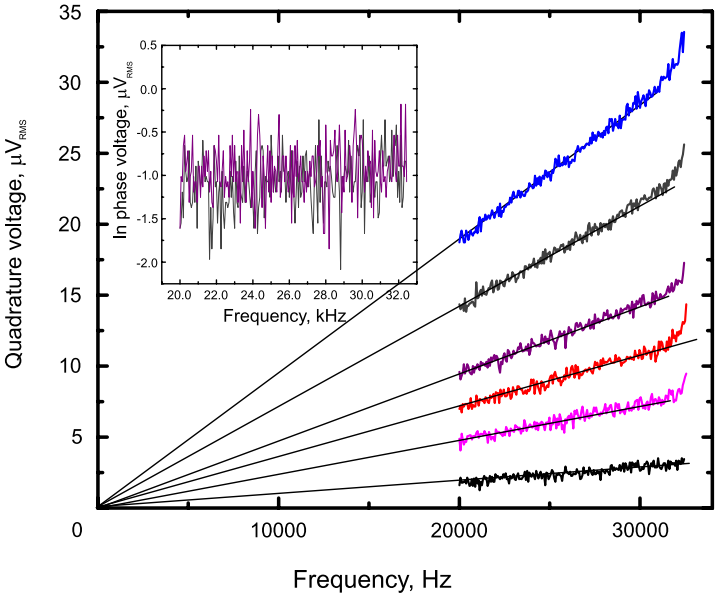

Fig. 8 (Color online) Frequency dependence of the quadrature component of the voltage V measured in vacuum and at temperature of 4 K for various excitation voltages V_g (100, 200, 300, 400, 600 and 800 mV_{RMS}) attenuated by −60 dB. The lines represent the fit to the experimental data by (24). The rise of the signal in the frequency range above 30 kHz is the onset to the fork resonance. The *inset* shows the dependence of the in-phase component measured at the same time as the quadrature one, showing small negative offset due to the presence of another capacitively coupled voltage source (for details see text)

in the frequency range below the fork resonance frequency (the fork motion is usually damped in an experiment and thus, the resonance frequency decreases). To show a comparison of the model presented above with experimental results, the voltage backgrounds for a fork were measured at a temperature of 4 K in vacuum.

The current flowing through the fork was measured using a home made I/V convertor with an adjustable gain factor of 10^3, 10^4 and 10^5, set by the value of R_F, i.e. $R_F = 1\ \mathrm{k}\Omega$, $10\ \mathrm{k}\Omega$ and $100\ \mathrm{k}\Omega$, respectively [16]. In the following discussion, as R_F comes directly into the measured signal (see (22) and (23)), the gain will be stated directly in terms of R_F. The I/V convertor has input impedance $R_i \to 0\ \Omega$ and except for the tuning fork, the only resistance connected to its input was the resistance of the coaxial cable of the order of few ohms. Special attention was paid to have as good ground connections as possible in order to eliminate the problems discussed above.

The inset of Fig. 8 shows the frequency dependence of the in-phase component measured for various excitations attenuated by −60 dB. The phase of the reference signal for the lock-in amplifier in all measurements presented below was set to 180°. As one can see, there is a 1 μV negative shift of the in-phase component amplitude, which within measurement sensitivity does not depend on the excitation amplitude. This amplitude dependence is in contradiction to the model presented. However, one can also assume that this negative voltage shift may be caused by the generator synchronization output working as another voltage source capacitively coupled to the tuning fork. Thus, the fork is excited from two voltage sources: the primary, directly

coupled voltage source and the second one, capacitively coupled source formed by the synchronization output of the generator (to present a simple model this possibility was not taken into account).

The I/V converter gain was 100 kΩ and 1 μV negative shift of the in-phase component corresponds to a current of the order of 10 pA, the value of which is mainly determined by the impedance of this coupling capacitance. If the synchronization pulse amplitude is approximately 3 volts, then the estimated value of the coupling capacitance is of the order of 20 aF.

The presence of this capacitively coupled source supplying the tuning fork can be detected especially, when the tuning fork has Q factor of the order of 10^6 or higher. Such a fork is measured with a very tiny excitation, which is comparable with that passing through the capacitive coupling between the synchronization output and the tuning fork. Then the fork current–voltage dependence, from which the α constant is determined, will not cross the zero point on the current axis and the phase of the measured current will be shifted from 90° to zero (or 180°) as the excitation voltage from the primary source becomes dominant.

Based on the discussion above we may assume that there is a negligible influence of the in-phase component to the background voltage V_{bgrd} i.e. $R_i \to 0\ \Omega$, $R_1 \to 0\ \Omega$ and $\bar{k} \to 1$, and therefore, the frequency dependence of the background voltage (see (22)) can be simplified as

$$V_{bgrd} = -i\omega R_F C V_g(\omega). \tag{26}$$

Figure 8 shows the frequency dependencies of the quadrature component of the current measured for various excitations. The signals are positive due to the 180° phase shift of the reference signal. The expected linear dependence in frequency, with different slopes ($R_F C V_g$) due to various excitations V_g, allows the value of the fork shunt capacitance C to be determined. Figure 9 presents the linear dependence of the values ($R_F C V_g$) as a function of V_g. As the I/V converter gain was $R_F = 100$ kΩ, from the fit to the experimental data follows that the fork shunt capacitance is 2 pF. Inset to Fig. 9 shows a linear dependence of $R_F C V_g$ determined from the frequency sweeps at constant excitation voltage V_g, but for different gains of the I/V converter, R_F. This measurement confirms the value of the fork shunt capacitance to be 2 pF.

Regarding the compensation circuit, shown in Fig. 7, this was found to operate as expected. As a variable capacitor we used just an ordinary mechanical capacitance trimmer (one can design this circuit in a more sophisticated way allowing a fine compensation using a varicap) and the invertor can be made of any low noise type operational amplifier.

8 Torsional Oscillators and Grids

Torsional oscillators and electrostatically driven grids are other examples of oscillating devices, which generate a current due to their motion. Forced oscillatory motion of these devices, in the linear approximation, is described by the same as that for the tuning fork motion (see (18)).

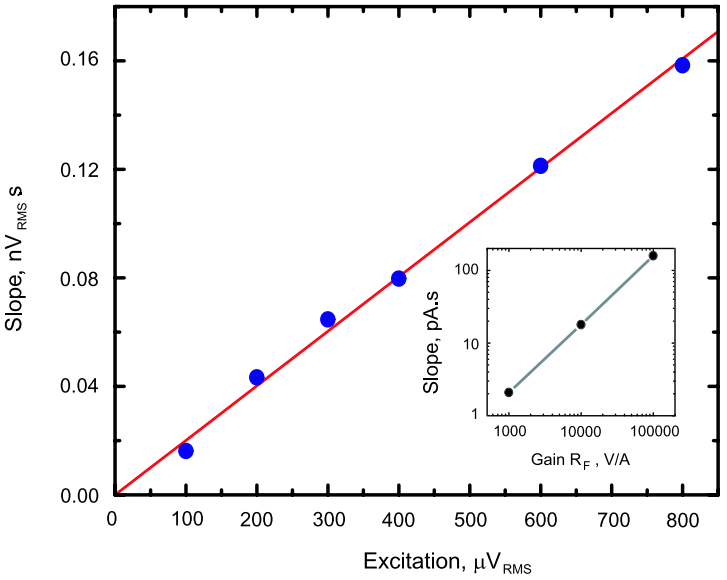

Fig. 9 (Color online) The values of slopes ($R_F C V_g$) as a function of the various excitation voltages V_g. The *line* represents the fit to experimental data using linear dependence, from which the value of the shunt capacitance C can be determined. The *inset* shows a similar dependence measured at constant excitation voltage V_g but for the different gains of the I/V converter. The slope of the linear function allows to determine the value of the fork shunt capacitor C again

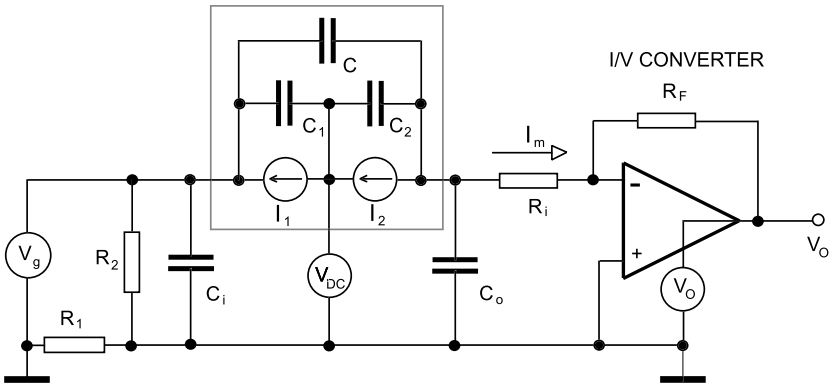

Fig. 10 Schematic electric connection of a typical circuit used for torsional oscillator and grid measurements. The motion of the torsional oscillator and grid can be modelled as frequency dependent current sources I_1 and I_2, which when driven the amplitudes of those depend on excitation voltage V_g

A typical experimental setup used for grids/torsional oscillators measurements is presented in Fig. 10. Two fixed electrodes form a capacitor with the capacitance C. A movable electrode placed between the fixed electrodes creates another two capacitors, C_1 and C_2 with distances d_1 and d_2, respectively, between the electrodes. This third electrode, in the case of the grid, is the grid itself. In the case of a torsional os-

cillator the moving electrode is mechanically connected to the cylindrical body of the oscillator. A DC source V_{DC} connected to the moving electrode generates a constant electric field between this electrode and the fixed electrodes. This electric field is harmonically modulated by the voltage $V_g(\omega)$ from the generator. When the frequency of the modulation field is the same as the resonance frequency of the mechanical motion of the grid/torsional oscillator, the resonance condition is achieved.

In both cases, the displacement of the motional electrode produces time variation in the capacitances C_1 and C_2, and this generates the currents I_1 and I_2

$$I_1(\omega) = V_{DC}\frac{dC_1}{dt} = -V_{DC}\frac{C_1}{d_1}v(\omega), \qquad I_2(\omega) = V_{DC}\frac{dC_2}{dt} = -V_{DC}\frac{C_2}{d_2}v(\omega) \tag{27}$$

where $v(\omega)$ is given by expression (2) and we assumed that $V_{DC} \gg V_g$. The currents I_1 and I_2 are opposite to each other and frequency (and excitation) dependent. The amplitude of the harmonic driving force for this type of mechanical resonators can be expressed as

$$F = \frac{C_1 V_{DC}}{d_1} V_g(\omega). \tag{28}$$

Similar to the fork analysis, the voltage detected by the I/V converter consists of two contributions expressed by (21). Using the superposition theorem one can get an expression for V_{bgrd} in the form

$$V_{bgrd} = -\frac{Z_2}{R_1 + Z_2}\frac{1}{1+\omega^2\bar{C}_0^2R_i^2}\left(\omega^2 R_F R_i C\bar{C}_0 - \frac{R_1}{Z_2} + i\bar{k}\omega R_F C\right)V_g(\omega), \tag{29}$$

which is the same equation as for the fork (see (22) with the small difference that $\bar{C}_0 = C_0 + C_2$ and $Z_2 = R_2/(1 + i\omega R_2\bar{C}_i)$, where $\bar{C}_i = C_i + C_1$. Similarly, for the signal voltage one can get

$$V_{sig}(\omega) = -\frac{1 - i\omega\bar{C}_0R_i}{1+\omega^2\bar{C}_0^2R_i^2}R_F I_2(\omega) = I_m(\omega)R_F. \tag{30}$$

Here only the source $I_2(\omega)$ contributes to the output voltage because the source $I_1(\omega)$ is separated from the output: shorted by the voltage sources V_g and V_{DC}. In principle, the same rules applicable for the tuning fork measurements are adaptable to the grid/torsional oscillator as well.

9 Torsional Oscillators and Grids—Experimental

To compare the model presented above to experiments a grid was used having the resonance frequency at 926 Hz and Q-factor in vacuum of the order of 10^5 [17, 18]. Measurements were performed in superfluid ^{4}He at a temperature of 100 mK. The current generated by the grid motion was detected by a current to voltage converter with $R_i \to 0\ \Omega$ [16] and the only input resistance was the resistance of the coaxial

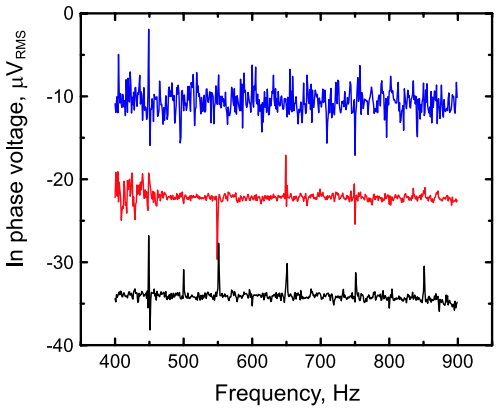

Fig. 11 (Color online) Frequency dependence of the in-phase voltage measured for three excitations (9, 18 and 27 mV_{RMS}). Non-zero values of in-phase voltage suggest a presence of a potential difference between the generator ground and the I/V converter ground

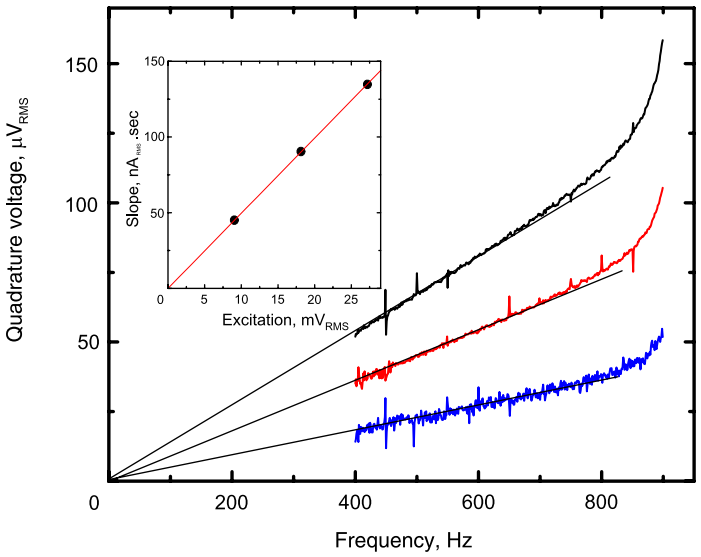

Fig. 12 (Color online) Frequency dependence of the quadrature voltage measured for three different excitations (9, 18 and 27 mV_{RMS}). The rise of the signal in the frequency range above 800 Hz is the onset to the grid resonance. The *inset* shows the expected linear dependence of the $kR_2CV_g/(R_1+R_2)$ values on excitation voltage V_g

cable connected between the grid and the I/V converter. The converter gain factor was 10^5 V/A. As $R_i \to 0\ \Omega$ and $Z_2 \simeq R_2$, the expression (29) can be rewritten as

$$V_{bgrd} = -\frac{R_2}{R_1+R_2}\left(-\frac{R_1}{R_2} + i\bar{k}\omega R_F C\right) V_g(\omega). \tag{31}$$

Figure 11 shows the in-phase component as a function of the frequency measured for various excitations. To obtain a positive signal from the grid, the phase of the reference signal was shifted by 180° and due to this the background signal of the in-phase component is negative. Results presented in Fig. 11 suggest the presence of

a potential difference between the generator and the I/V converter grounds (the first term in expression (31)).

Figure 12 presents the quadrature component. At low frequencies the amplitude of the quadrature component increases linearly with frequency and for frequency $\omega \to 0$ rad/sec this signal amplitude passes through zero. The lines represent fit to the experimental data using the second, imaginary term of expression (31). At higher frequencies, due to the high Q value of the grid, the onset to the resonance is seen. The inset of Fig. 12 shows a linear dependence of the slopes $\bar{k}R_2CV_g/(R_1 + R_2)$ divided by R_F (the I/V converter gain 10^5) from which the value $\bar{k}R_2C/(R_1 + R_2)$ can be determined, where $\bar{k} = 1 - R_1\bar{C}_0/(R_2C)$. To eliminate a problem with the determination of $\bar{k}$ value, it is important to reduce the potential difference between the I/V converter and the source of the excitation to zero value, that is $R_1 \to 0\ \Omega$, then $\bar{k} = 1$ and one can determine experimentally the value of the capacitance C. It is worth to note at this point that results presented for the grid are in qualitative agreement only.

10 Conclusion

In conclusion an analysis of the influence of the various electronic circuitries, together with their contributions to the measurement backgrounds of the traditional mechanical vibrating resonators like vibrating wires, tuning forks and grids using simple models was presented and compared with experiments. These simple models show a reasonable agreement with experimental reality and allow to extract the useful experimental information about circuitry, and in such a way to help to understand better the physical problems investigated using these mechanical resonators at low temperatures.

Acknowledgements Finally, I would like to acknowledge colleagues who shared their experience of using these oscillating tools with me: D.I. Bradley, M. Človečko, V. Efimov, S.N. Fisher, D. Garg, E. Gažo, A.M. Guénault, R.P. Haley, S. Holt, M. Jackson, P.V.E. McClintock, G.R. Pickett, R. Schanen, L. Skrbek, V. Tsepelin and L. Wheatland. Centre of Low temperature Physics is operated as the Center of Excellence of the APVV and the Slovak Academy of Sciences and P.J. Šafárik University under contracts VVCE-0058-07 and CE I-2/2007, respectively. This work is supported by the grants: APVV-0432-07, APVV-0346-07, VEGA 2/0025/09, EPSRC and by Microkelvin, the project of 7. FP of EU. Support provided by the U.S. Steel Košice s.r.o. is also very appreciated.

References

1. S.N. Fisher, A.M. Guénault, C.J. Kennedy, G.R. Pickett, Phys. Rev. Lett. **63**, 2566 (1989)
2. M.P. Enrico, S.N. Fisher, A.M. Guénault, G.R. Pickett, K. Torizuka, Phys. Rev. Lett. **70**, 1846 (1993)
3. S.N. Fisher, A.J. Hale, A.M. Guénault, G.R. Pickett, Phys. Rev. Lett. **86**, 244 (2001)
4. E. Collin, L. Filleau, T. Fournier, Y.M. Bunkov, H. Godfrin, J. Low Temp. Phys. **150**, 739 (2008)
5. G.W. Morley, A. Casey, C.P. Lusher, B. Cowan, J. Saunders, J.M. Parpia, J. Low Temp. Phys. **126**, 557 (2002)
6. J. Jager, B. Schuderer, W. Schoepe, Phys. Rev. Lett. **74**, 566 (1995)
7. D.O. Clubb, O.V.L. Buu, R.M. Bowley, R. Nyman, J.R. Owers-Bradley, J. Low Temp. Phys. **136**(1–2), 1 (2004)

8. R. Blaauwgeers, M. Blažková, M. Človečko, V.B. Eltsov, R. de Graaf, J.J. Hosio, M. Krusius, D. Schmoranzer, W. Schoepe, L. Skrbek, P. Skyba, R.E. Solntsev, D.E. Zmeev, J. Low Temp. Phys. **146**(5–6), 537 (2007)
9. M. Blažková, M. Človečko, V.B. Eltsov, E. Gažo, R. de Graaf, J.J. Hosio, M. Krusius, D. Schmoranzer, W. Schoepe, L. Skrbek, P. Skyba, R.E. Solntsev, W.F. Vinen, J. Low Temp. Phys. **150**, 525 (2008)
10. A.P. Sebedash, J.T. Tuoriniemi, E.M. Pentti, A.J. Salmela, J. Low Temp. Phys. **150**, 181 (2008)
11. E.M. Pentti, J.T. Tuoriniemi, A.J. Salmela, A.P. Sebedash, J. Low Temp. Phys. **150**, 555 (2008)
12. D.I. Bradley, J. Hayes, J. Low Temp. Phys. **119**(5–6), 703 (2000)
13. J. Martikainen, J. Tuoriniemi, J. Low Temp. Phys. **124**, 367 (2001)
14. http://www.cmr-direct.com/
15. R.D. Grober, J. Acimovic, J. Schuck, D. Hessman, P.J. Kindlemann, J. Hespanha, S. Morse, K. Karrai, I. Tiemann, S. Morse, Rev. Sci. Instrum. **71**, 2776 (2000)
16. S. Holt, P. Skyba, to be published
17. D. Garg, V.B. Efimov, P.V.E. McClintock, private communications
18. V.B. Efimov, D. Garg, M. Giltrow, P.V.E. McClintock, L. Skrbek, W.F. Vinen, J. Low Temp. Phys. **158**, 462 (2010)